ACS OMEGA

http://pubs.acs.org/journal/acsodf

Article

Ag_3PO_4/NiO Composites with Enhanced Photocatalytic Activity under Visible Light

Ricardo K. Santos, Tiago A. Martins, Gabriela N. Silva, Marcus V. S. Conceição, Içamira C. Nogueira, Elson Longo, and Gleice Botelho*

Cite This: *ACS Omega* 2020, 5, 21651−21661

Read Online

ACCESS | Metrics & More | Article Recommendations | Supporting Information

ABSTRACT: Black NiO powders were prepared by a hydrothermal method. Moreover, the visible light-driven Ag_3PO_4/NiO photocatalyst composites were successfully synthesized by in situ precipitation method. These samples were structurally characterized by X-ray diffraction and Rietveld refinement. The strong interaction between the phases and the defects in the samples was affected by the formation of the composites, as identified by Fourier transform infrared spectroscopy and Raman spectroscopy. UV−vis diffuse reflectance spectroscopy exhibited enhanced light absorption for all Ag_3PO_4/NiO composites, suggesting the effective interaction between the phases. Moreover, field-emission scanning electron microscopy images revealed the presence of NiO microflowers composed of nanoflakes in contact with Ag_3PO_4 microparticles. The composite with 5% NiO presented enhanced photocatalytic efficiency in comparison with pure Ag_3PO_4, degrading 96% of rhodamine B (RhB) dye in just 15 min under visible light; however, the recycling experiments confirmed that the composite with 75% NiO showed superior stability. The recombination of the electron−hole pairs was considered for the measurement of the photoluminescence of the samples. These measurements were performed to evaluate the possible causes for the difference in the photocatalytic responses of the composites. From these experimental results, possible photocatalytic mechanisms for RhB degradation over Ag_3PO_4/NiO composites under visible-light irradiation were proposed.

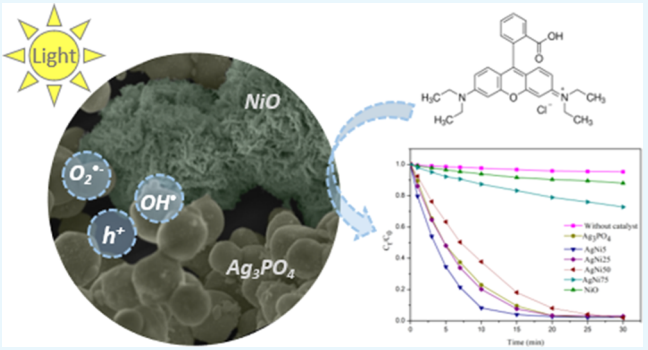

INTRODUCTION

Photocatalysts with potential for solving environmental problems using visible-light irradiation have been extensively studied. Among the studied photocatalysts, silver phosphate (Ag_3PO_4) has attracted considerable attention since it was discovered by Yi et al.[1] in 2010. Its narrow band gap of ∼2.4 eV enables the use of visible-light radiation that represents approximately 43% of the solar spectrum. Therefore, Ag_3PO_4 is a promising candidate for application in visible light-driven photocatalysts primarily for the degradation of organic pollutants and water splitting.[2−6] Since the discovery of the Ag_3PO_4 semiconductor, many mechanisms such as cation/anion doping, composite construction, metal deposition, and immobilization with support materials have been studied to increase its stability and photocatalytic properties.[3,4,7−9]

The formation of a composite by coupling Ag_3PO_4 with other semiconductors is a widely used strategy to enhance the visible-light response, improve the separation of electron−hole pairs, suppress their recombination, and enhance the stability. Recently, Guo et al.[10] prepared Ag_3PO_4/AgCl by an in situ precipitation method, showing an enhanced photocatalytic activity for the degradation of parabens compared with pure Ag_3PO_4 and AgCl. Shaveisi and Sharifnia[11] have reported the synthesis of Ag_3PO_4/CaO as an efficient visible light-driven heterojunction photocatalyst for the degradation of ammonia from wastewater. Other recent studies have reported coupling Ag_3PO_4 with CuO,[12] $MgFe_2O_4$,[13] WO_3,[14] MoS_2,[15] and $In(OH)_3$.[16] Therefore, the suitable adjustment of the band-energy levels in the two semiconductors of a composite photocatalyst effectively generates new materials with increased photocatalytic efficiency. These new materials can be utilized to control environmental problems.

NiO is a relatively low-cost and low-toxicity material with high chemical/thermal stability and has been utilized in various fields involving photocatalysts, lithium-ion batteries, magnetic materials, adsorbents, electrochromic devices, and gas sensors.[17−22] The photocatalytic properties of NiO have been utilized for the degradation of organic pollutants such as methylene blue and rhodamine B (RhB).[22−24] These studies

Received: May 25, 2020
Accepted: July 31, 2020
Published: August 17, 2020

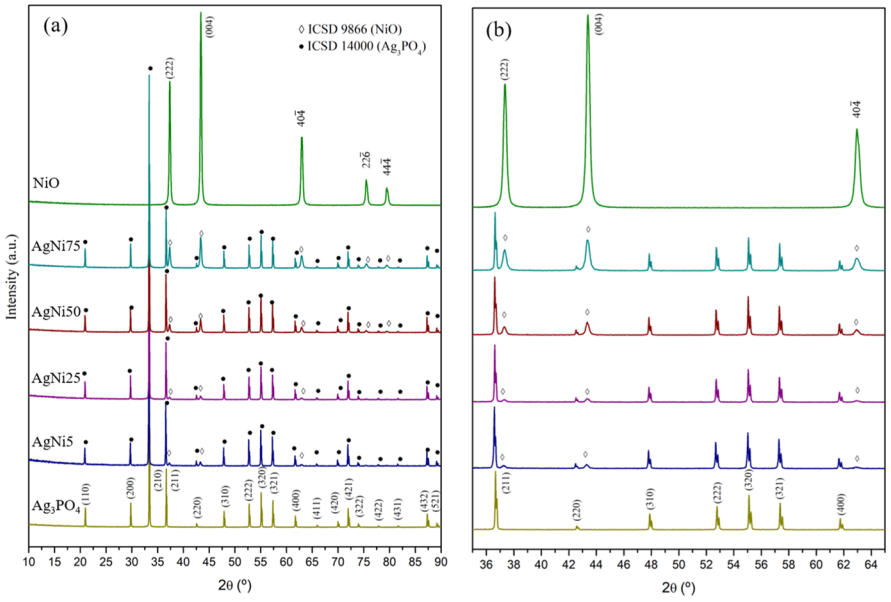

Figure 1. (a) XRD patterns of the powders and (b) magnified XRD patterns in the range from 35 to 65°.

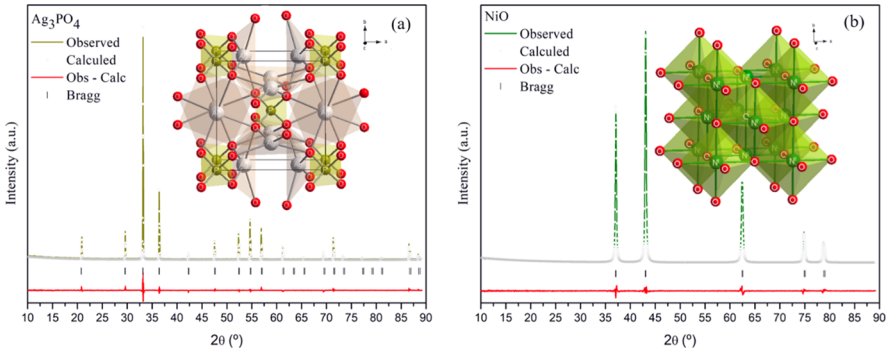

Figure 2. Rietveld refinement plots of (a) Ag_3PO_4 and (b) NiO samples.

were performed under UV irradiation because the wide band gap of NiO (approximately 3.6−4.0 eV) impedes the photocatalytic activity under visible light. Additionally, the rapid recombination of the electron−hole pairs is reportedly another disadvantage that limits the efficiency of NiO.[23,25,26]

However, the performance of NiO can be optimized by controlling the synthesis conditions, generating NiO samples with different amounts of defects (vacancies), colors, surface areas, morphology, and visible-light responses.[23,27−29] For example, Liu et al.[28] synthesized black NiO by a hydrothermal method and calcined it at 500 °C for 2 h in air. The sample presented a narrowed band gap of ∼1.42 eV and a wide light-absorption region. Recently, Baygi et al.[29] prepared highly porous NiO powders by solution combustion synthesis. These dark green samples exhibited band gaps of 1.8 eV as well as wide visible-light absorption. The results of the photocatalytic experiments under sunlight with methylene blue as the dye showed the potential of the NiO powders. Therefore, NiO with a narrow band is a possible candidate for coupling with Ag_3PO_4. To the best of our knowledge, there is no available report on the synthesis, characterization, and application of Ag_3PO_4/NiO composites.

In this paper, we report the synthesis of Ag_3PO_4/NiO by coupling of Ag_3PO_4 with black NiO through a simple in situ precipitation method and investigate its application for the degradation of RhB dye. The effects of the NiO content in the composites on the photocatalytic efficiency and stability were also investigated. The mechanism responsible for the photocatalytic degradation of RhB over the Ag_3PO_4/NiO composite was discussed in detail.

RESULTS AND DISCUSSION

X-ray Diffraction and Rietveld Refinements. Figure 1a shows the X-ray diffraction (XRD) patterns of pure samples (NiO and Ag_3PO_4) and Ag_3PO_4/NiO composites. The diffraction peaks of Ag_3PO_4 sample were well indexed to the body-centered cubic structure with space group $P\bar{4}3n$, in agreement with Inorganic Crystal Structure Database (ICSD) no. 14000.[30] Similarly, the NiO diffractogram was perfectly indexed to the face-centered cubic structure with space group $Fm\bar{3}m$ (ICSD no. 9866).[31] In the composite samples, it is possible to observe the main diffraction peaks from Ag_3PO_4 and NiO. Furthermore, it is notable that the relative intensity diffraction of the peaks of NiO gradually increased with increasing NiO content (Figure 1b). However, when the amount of NiO was lower than 50% (AgNi5 and AgNi25), low-intensity diffraction peaks of NiO, corresponding to the $(22\bar{6})$ and $(44\bar{4})$ planes, were not observed. Moreover, the addition of NiO does not change the diffraction peak positions of Ag_3PO_4 in the Ag_3PO_4/NiO composites when compared

https://dx.doi.org/10.1021/acsomega.0c02456
ACS Omega 2020, 5, 21651−21661

with ICSD no. 14000. This suggests that NiO did not incorporate into the lattice of Ag_3PO_4. Therefore, these experimental results show that no impurity peaks were detected in the XRD patterns, indicating that the Ag_3PO_4, NiO, and Ag_3PO_4/NiO powders were successfully synthesized.

The Rietveld refinements were performed using the general structure analysis system (GSAS) software package with the EXPGUI graphical interface, to calculate the atomic positions, lattice parameters, and unit cell volumes of these samples. In these analyses, the refined parameters were background, scale factor, shift lattice constants, profile half-width parameters (u, v, w), isotropic thermal parameters, lattice parameters, strain anisotropy factor, preferential orientation, and atomic functional positions. The background was modeled using the shifted Chebyshev polynomial of the first kind. The peak profile function was modeled using a convolution of the Thompson−Cox−Hastings pseudo-Voigt with the asymmetry function described by Finger.[32]

The Rietveld refinements confirmed that the Ag_3PO_4 and NiO have body-centered cubic and face-centered cubic structures, respectively, without secondary phases. The refinements showed good correlation between experimentally observed and calculated XRD patterns, as illustrated by the line (Obs − Calc) (Figure 2a,b). Moreover, low deviations of the statistical parameters (R_{wp}, R_p, and χ^2) were observed (Table 1), indicating the reliability of the results. The lattice parameters and unit cell volume of the pure samples are also listed in Table 1, showing good agreement with those published in the literature.[27,33−35] However, an increase in the cell volume and lattice parameters was observed when compared with ICSD no. 14000[30] and no. 9866.[31] This behavior is usually associated with the synthesis method that generates various types of structural defects, such as vacancies and local lattice disorders.[33,35,36] For NiO, Maniammal et al.[36] associated the lattice expansion observed with the presence of defects and large surface area. A similar lattice expansion was reported in the black NiO nanoparticles with a high concentration of defects.[35] More details from the Rietveld refinements are provided in the Supporting Information (Tables S1 and S2). The Rietveld results for the Ag_3PO_4/NiO composites are presented in the Supporting Information (Figure S1 and Table S3), and the statistical parameters indicate that the quality of structural refinement data is acceptable. Significative variations in the lattice parameters and unit cell volumes were not observed in the composites, which are in good agreement with the pure samples.

Table 1. Rietveld Refinement Parameters of Ag_3PO_4 and NiO Samples

samples	lattice parameter a (Å)	cell volume (Å^3)	R_{wp} (%)	R_p (%)	χ^2
Ag_3PO_4	6.043(4)	220.724(0)	12.56	9.19	1.359
NiO	4.209(8)	74.612(0)	8.01	5.40	1.137
Ag_3PO_4 ICSD 14000	6.026 (5)	218.82			
NiO ICSD 9866	4.178 (1)	72.93			

The Rietveld refinement results were inserted as input data in the molecular and crystal structure visualization (Diamond) software to model the typical Ag_3PO_4 and NiO structures, as demonstrated in the insets of Figure 2. As observed in the modeled structure for Ag_3PO_4, both Ag and P atoms are coordinated to four oxygen atoms, resulting in tetrahedral [AgO_4] and [PO_4] clusters. Regarding the NiO structure, the Ni atoms are coordinated to six oxygen atoms, resulting in octahedral clusters.

Fourier Transform Infrared and Micro-Raman Spectroscopies. Fourier transform infrared spectroscopy (FTIR) and Raman analysis were performed to provide information on the chemical structure of the samples. FTIR spectra obtained for all samples are shown in Figure 3a. All samples presented a broad vibrational band around 3400 cm^{-1} related to the O−H stretching vibrations of adsorbed water molecules on the samples. In the NiO sample, the appearance of a strong absorption band at 425 cm^{-1} is attributed to the Ni−O stretching vibrations.[22,27] Ag_3PO_4 presented typical vibrational bands related to the PO_4^{3-} group. For example, symmetric P−O stretching vibration bands were detected at 989 and 859 cm^{-1}, P−O asymmetric stretching vibrations were found at 1075 cm^{-1}, asymmetric stretching vibrations of the PO_4^{3-} group were located at 1407 cm^{-1}, and P−O−P bending vibrations were present at 547 cm^{-1}. Moreover, the Ag_3PO_4 sample presented a vibrational band at 1657 cm^{-1} attributed to the H−O−H bending vibrations of adsorbed water molecules.[6,37,38] In addition, characteristic bands of both NiO and Ag_3PO_4 powders can be observed in the Ag_3PO_4/NiO composites, and the relative intensity of the bands of NiO increases with increasing NiO content in the composites. These FTIR spectra confirm the absence of any impurities in the samples. Moreover, the characteristic peaks of Ag_3PO_4 in the Ag_3PO_4/NiO composites are slightly shifted, primarily for AgNi25, AgNi50, and AgNi75, which can be attributed to the interaction between the Ag_3PO_4 and NiO phases.[15,39,40]

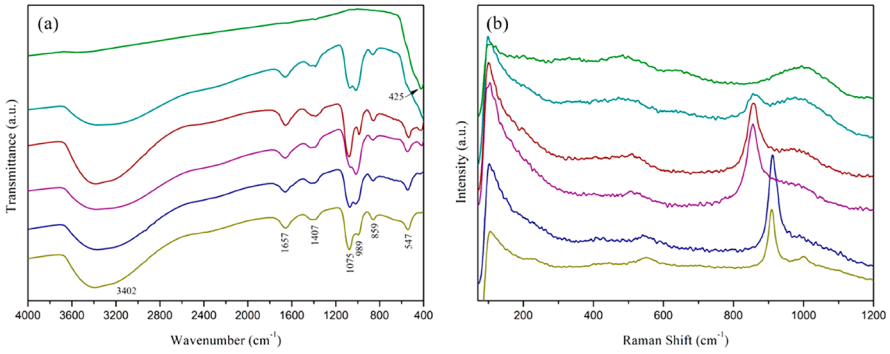

Figure 3. (a) FTIR and (b) Raman spectra of the samples.

https://dx.doi.org/10.1021/acsomega.0c02456
ACS Omega 2020, 5, 21651−21661

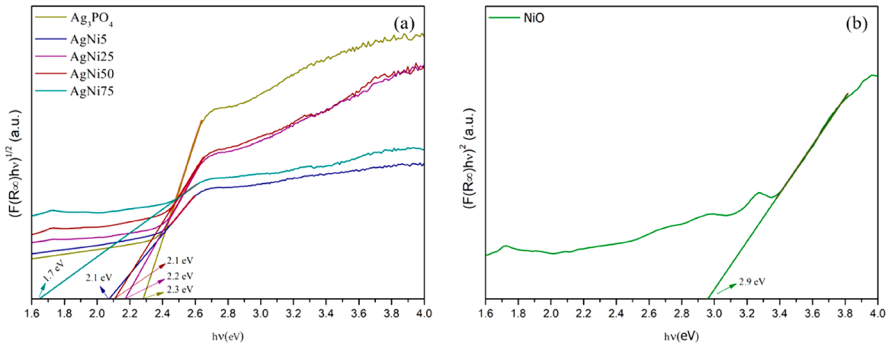

Figure 4. Tauc equation applied to DRS spectra to obtain band gap values for (a) Ag_3PO_4 and Ag_3PO_4/NiO composites and (b) NiO.

The Raman spectra obtained for all samples are shown in Figure 3b. According to first-principles calculations previously published,[34] Ag_3PO_4 presents a total of 18 Raman-active modes; however, in this work, only five Raman-active modes were identified, all related to $[PO_4]$ clusters. For example, the absorption bands at 909 and 999 cm^{-1} can be attributed to the symmetric and asymmetric stretching vibrations of O−P−O bonds, respectively, while the absorption band at 551 cm^{-1} can be attributed to the asymmetric bending vibrations of the $[PO_4]$ clusters. Finally, the absorptions related to rotation and translation of this cluster were identified at 103 and 229 cm^{-1}.

For the NiO sample, the broad band in the range of 400−600 cm^{-1} is associated with the overlapping of the transverse optical (TO) phonon mode and the longitudinal optical (LO) phonon mode. Moreover, a broad band at ∼1005 cm^{-1} and a weak band at ∼670 cm^{-1} can be attributed to the 2LO and 2TO modes, respectively. The presence of first-order TO and LO modes can be attributed to the presence of defects in the NiO, such as Ni^{2+} vacancies, because these modes are not observed in stoichiometric NiO. For example, Gandhi and Wu[35] observed enhanced intensity of the LO mode for black NiO nanoparticles, where the Ni vacancy concentration was high. Therefore, in this work, the Raman-active modes are in agreement with the previous reports regarding the NiO phase and indicate the presence of Ni^{2+} vacancies introduced by controlling the synthesis conditions and calcination temperature, resulting in a non-stoichiometric NiO.[36,41]

In the Ag_3PO_4/NiO composites, the main characteristic bands of both Ag_3PO_4 and NiO were observed. However, it is possible to clearly observe that the band of Ag_3PO_4 at 909 cm^{-1} is strongly shifted in the AgNi25, AgNi50, and AgNi75 composites. For AgNi5, this displacement is not observed; however, this sample presents less defined bands than those of Ag_3PO_4. This behavior observed by the composites is usually attributed to the strong interaction between the phases or lattice distortion and structural defects.[42−44] Thus, the in situ formation of Ag_3PO_4 may have contributed to the formation of defects (bulk, surface, and interface) in the composites. These results are in good agreement with the FTIR analysis.

UV−Visible Diffuse Reflectance Spectroscopy. The optical properties were analyzed by UV−vis diffuse reflectance spectroscopy (DRS), as the ability to absorb light directly influences the photocatalytic activity of the semiconductors. The insets in Figure S2 (Supporting Information) show different colors (left to right) corresponding to Ag_3PO_4, AgNi5, AgNi25, AgNi50, AgNi75, and NiO. The colors of the powders indicate the differences among the optical properties of these materials. In this figure, it is possible to observe the UV−vis DRS spectra of the pure samples and Ag_3PO_4/NiO composites. The Ag_3PO_4 presented a decrease in the reflectance at approximately 500 nm because of its strong absorption in the visible spectrum. Meanwhile, NiO presented a low reflectance spectrum in the entire visible region because of its black color (see the digital photo in the inset of Figure S2). For this sample, it is possible to observe three weak absorptions between 320, 387, and 720 nm. The absorptions of NiO are primarily associated with the d−d transitions of Ni^{2+} ions in an octahedral environment.[35,36,45] In addition, the black color of the NiO powders is usually attributed to the presence of Ni^{2+} vacancies, which lead to the formation of Ni^{3+} ions to acquire charge neutrality. Hence, the presence of Ni^{2+} vacancies induces lattice defects, and intermediate energy levels are introduced into the non-stoichiometric NiO, which results in a decrease in the band gap energy.[28,35,45,46] Therefore, these observations are in agreement with the previous results. In all composites, it is possible to observe the characteristic absorption of Ag_3PO_4 and NiO, with small variations in the absorption wavelengths.

The band gap energy (E_{gap}) values were estimated using the Tauc equation:[47] $\alpha h\nu = A(h\nu - E_{gap})^n$, where h is the Planck constant, ν is the light frequency, α is the absorption coefficient, and A is a proportionality constant. The value of the exponent n denotes the type of semiconductor transition. According to the literature, the Ag_3PO_4 and NiO powders present indirect allowed ($n = 2$) and direct allowed ($n = 1/2$) electronic transitions, respectively.[6,23,28,45] Because α is proportional to the Kubelka−Munk (K−M) function,[48] the equation becomes: $(F(R_\infty)h\nu)^{1/n} = A(h\nu - E_{gap})$, where $F(R_\infty)$ is the K−M function or diffuse reflectance of the sample. Therefore, when plotting $(F(R_\infty)h\nu)^{1/n}$ against $h\nu$, E_{gap} corresponds to the $h\nu$ value at the intersection of the line tangent to the graph with the horizontal axis. The E_{gap} values obtained were 2.3, 2.1, 2.2, 2.1, 1.7, and 2.9 eV for Ag_3PO_4, AgNi5, AgNi25, AgNi50, AgNi75, and NiO, respectively, as shown in Figure 4a,b. The E_{gap} of the Ag_3PO_4 and NiO samples are in accordance with previous reports.[7,33,34,45,46] The band gap of the composites narrowed slightly as compared to that of Ag_3PO_4 with enhanced light absorption. Among the composites, AgNi75 showed the lowest band gap (E_{gap} = 1.7 eV), probably associated with the introduction of surface defects caused by the greater amount of NiO during the in situ precipitation of Ag_3PO_4, which can lead to a strong interaction between semiconductors, facilitating the formation of an interaction between the NiO and Ag_3PO_4 phases.[28,40]

Morphological Aspects. The morphologies of the pure samples and Ag_3PO_4/NiO composites were investigated by

https://dx.doi.org/10.1021/acsomega.0c02456
ACS Omega 2020, 5, 21651−21661

field-emission scanning electron microscopy (FE-SEM), as illustrated in Figure 5a−m. The left images are of low magnification, while the right images are of high magnification, showing the delimited region (white dashed square). The Ag_3PO_4 morphology (Figure 5a) demonstrated the formation of irregular spherical microparticles, with an average diameter of approximately 300 nm and high degree of aggregation (Figure 5b). The low-magnification FE-SEM image (Figure 5c) shows typical NiO composed of flower-like microparticles with an average diameter of approximately 3.5 μm and polydisperse nature (Figure 5c). Furthermore, from Figure 5c,d, it is possible to observe that the surface of NiO is not dense; the microflowers are formed by the self-assembly of several thin flake-like nanostructures, forming a 3D hierarchical structure with a highly porous texture. The inset of Figure 5d exhibits a magnified image of the surface of NiO, revealing that each nanoflake consists of aggregated interconnected nanoparticles with diameters of approximately 40 nm. A very similar morphology was obtained by Wang et al.,[49] who synthesized flower-like iron oxide nanostructures with the assistance of surfactants. The utilization of the surfactants served as a capping agent during the aggregation process. Moreover, these authors observed that the calcination temperature as well as the preparation time of precursors governed the morphology. In our work, urea was employed as a capping agent that promoted the self-assembly of the thin flake-like nanostructures to form the NiO microflowers. In addition, flower-like morphologies were observed in previous reports regarding NiO synthesized with several chemical synthesis methods, such as the precipitation method and solvothermal/hydrothermal routes. Therefore, NiO demonstrates a tendency to form flower-like morphologies.[17,21−23]

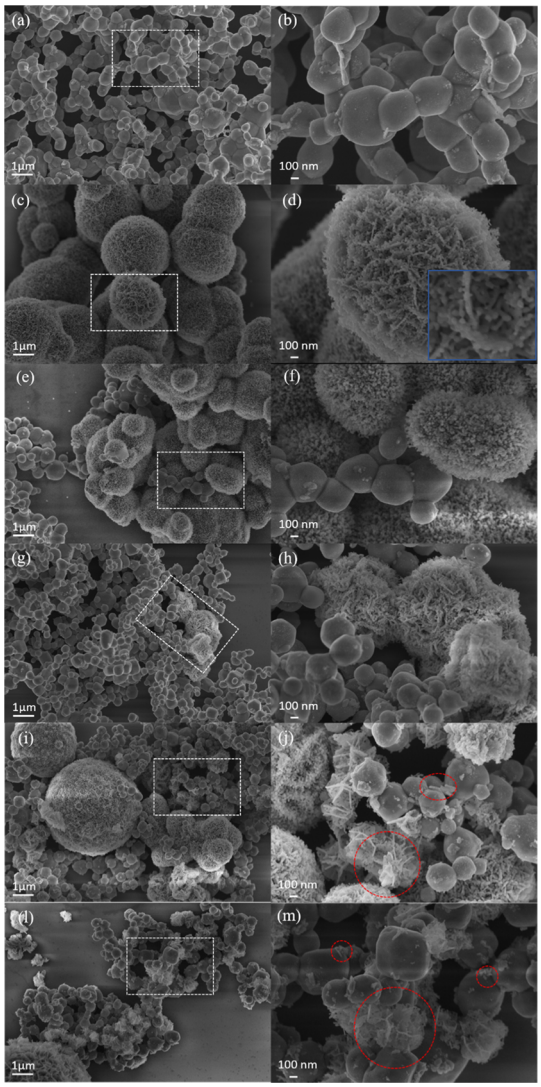

Figure 5. FE-SEM images of (a,b) Ag_3PO_4, (c,d) NiO, (e,f) AgNi5, (g,h) AgNi25, (i,j) AgNi50 and (l,m) AgNi75 powders.

All composites maintained the morphology of Ag_3PO_4, even after the precipitation in situ on NiO (Figure 5e−m). In the composites with a high amount of NiO (Figure 5i−m), it is possible to clearly observe a small assembly of flake-like nanostructures, which may correspond to the initial stage of formation of NiO microparticles, suggesting that the large NiO microflowers are formed from several aggregated flake-like nanostructures. Moreover, the FE-SEM micrographs show that Ag_3PO_4 microparticles are in contact with the NiO microflowers, and some nanoflakes of NiO are distributed on the Ag_3PO_4 surface (dashed red circles in Figure 5j,m), which is an indication of the formation of a contact surface between the Ag_3PO_4 and NiO phases. Then, the narrowed band gap observed for the AgNi75 composite may be associated with the large amount of NiO, which probably results in a greater interaction between semiconductors.

Photoluminescence, Photocatalytic Activity Test, Possible Photocatalytic Mechanism, and Durability. Photoluminescence (PL) was employed to investigate the mechanisms of the recombination of the electron−hole pairs and subsequently assist in the elucidation of the photocatalytic activity of the composites. Figure 6 shows the room-temperature PL spectra of the composites and pure samples. The pure Ag_3PO_4 samples exhibited a broad band with a maximum emission at ∼535 nm; the pure NiO samples exhibited a broad band covering the visible spectrum.

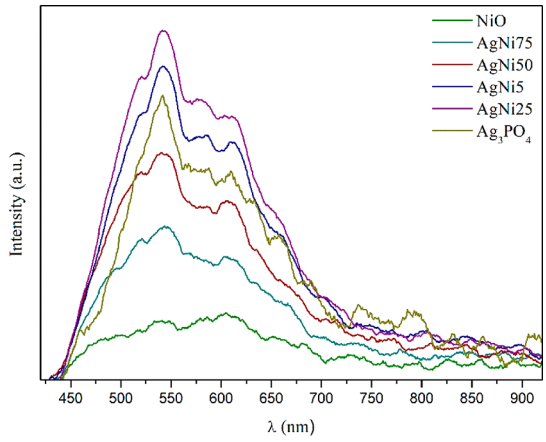

Figure 6. PL spectra of the samples.

The emission in the visible region was attributed to the presence of intrinsic defects in the NiO samples, which was corroborated by the results obtained from Rietveld, UV−vis DRS, FTIR, and Raman spectroscopies. This suggested the presence of Ni^{2+} vacancies.[23,35,36,42] The presence of other defects is also a possibility. Gandhi et al. studied the effect of the annealing temperature (400−800 °C) on the PL emission

https://dx.doi.org/10.1021/acsomega.0c02456
ACS Omega 2020, 5, 21651−21661

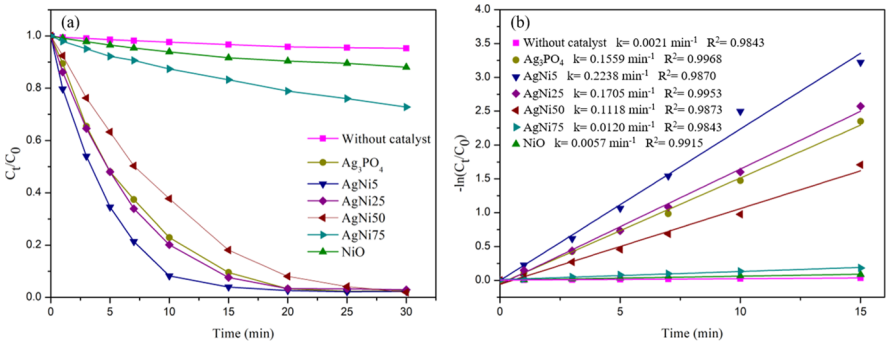

Figure 7. (a) Photocatalytic degradation and (b) kinetic fit curves for all samples under visible-light irradiation. *R^2 = correlation coefficient.

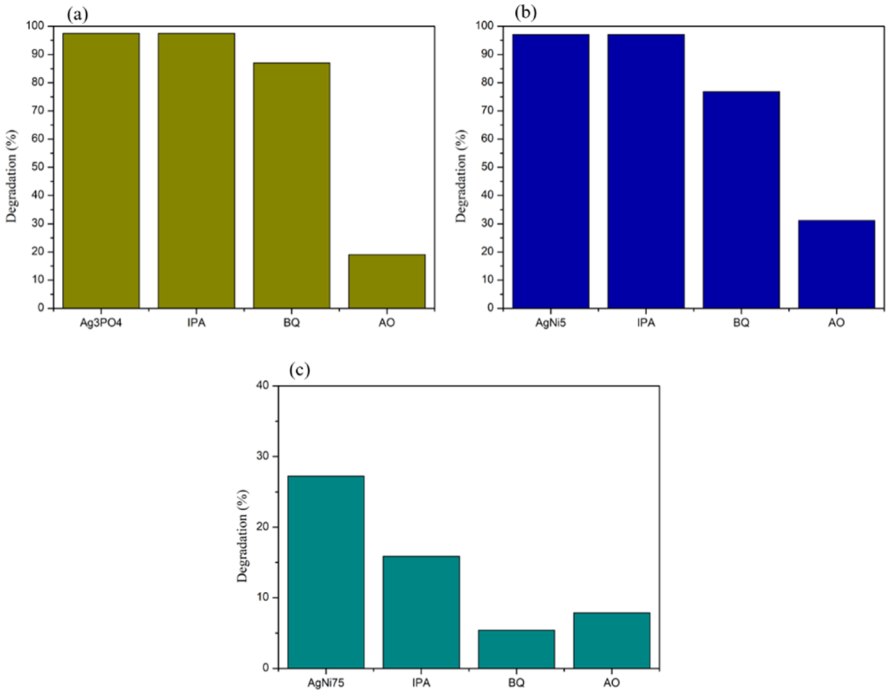

Figure 8. Effect of scavengers on the degradation efficiency of (a) Ag_3PO_4, (b) AgNi5, and (c) AgNi75.

spectra of the NiO samples. UV emission was suppressed in the samples that possessed a high concentration of defects; this was particularly prevalent in the samples that were annealed at 400 °C (black sample). The intense emission band that was exhibited by the sample at ∼520 nm was attributed to the presence of various structural defects such as oxygen vacancies and interstitial defects. This intense band was generated mainly due to the recombination of the electrons and photogenerated holes that were trapped in the shallow level below the conduction band (CB) and in the deep level oxygen vacancies, respectively. The characteristics of the PL emission spectra of the Ag_3PO_4 samples, corresponding to their band gap were ascribed to the radiative recombination of the electrons and holes in the CB and valence band (VB), respectively.[11,50] Apart from variations in the intensity, the spectra of the composites were similar to that of Ag_3PO_4.

Pure NiO and the composites with high amount of NiO (AgNi50 and AgNi75) exhibited a lower recombination rate; however, the PL intensity of the composites was higher than that of pure NiO. The intensity of the PL emission of the composites with high amount of Ag_3PO_4 (AgNi5 and AgNi25) was also higher than that of pure Ag_3PO_4. This suggested the formation of a type-I heterojunction (straddling gap), where NiO acted as a charge carrier donor for Ag_3PO_4 through interfacial charge carrier transfer to the CB of the Ag_3PO_4 semiconductor. This increased the photogeneration of the electron−hole pairs in Ag_3PO_4 of the Ag_3PO_4/NiO composites. Therefore, if the lifetime of charge carriers were longer than that of the photocatalytic reaction, degradation of RhB dye would be improved.[51−54]

The photocatalytic activity of the samples was evaluated by degradation of RhB solution under visible light. Figure 7a illustrates the discoloration curves (C_t/C_0), where C_0 and C_t are the initial and residual concentration of RhB at defined time (t) intervals, respectively. RhB was selected as a model pollutant because it is very resistant to light degradation, as demonstrated by the photolysis test, which showed a negligible degree of degradation after 30 min of exposure. In addition, only 12% of RhB was removed by pure NiO after irradiation for 30 min, while complete degradation of RhB was practically finished after irradiation for 20 min by pure Ag_3PO_4. It is known that pure NiO, when used as photocatalyst, presents rapid electron−hole recombination.[25] Hence, coupling NiO

https://dx.doi.org/10.1021/acsomega.0c02456
ACS Omega 2020, 5, 21651−21661

with Ag_3PO_4 can overcome this disadvantage and improve the photocatalytic activity.

The results clearly demonstrate that the addition of an appropriate amount of NiO to the composite enhanced the photocatalytic activity effectively in comparison with Ag_3PO_4. However, with a further increase in NiO content (>25%), the photocatalytic performance was decreased. Among the composites, AgNi5 exhibited the best photocatalytic performance, degrading 96% of RhB in only 15 min of exposure. AgNi25 and AgNi50 exhibited complete degradation after 20 and 25 min, respectively, while AgNi75 degraded only 27% after 30 min of irradiation. All photocatalytic tests were realized after 30 min in the dark to establish an adsorption−desorption equilibrium between the dye and photocatalyst, so that the observed results are due only to photocatalytic degradation.

The linear relationship between $-\ln(C_t/C_0)$ and t (Figure 7b) shows that the RhB degradation curves follow pseudo-first-order kinetics, described by $-\ln(C_t/C_0) = kt$, where k represents the reaction rate constant. The k values obtained for all samples are shown in Figure 7b. The rate constant of AgNi5 was 0.2238 min^{-1}, which is 1.4 times higher than that of Ag_3PO_4 (0.1559 min^{-1}).

Recent studies on the coupling of Ag_3PO_4 with other semiconductors have yielded promising results. Abroshan et al.[55] synthesized a $Ag_3PO_4/MnFe_2O_4$ nanocomposite with 30 wt % of $MnFe_2O_4$. The photocatalytic activity of this nanocomposite was evaluated by the degradation of RhB and methylene blue under light solar irradiation. The composites increased the efficiency of the reaction, with the reaction rate constant being approximately 1.5 times higher than that of pure Ag_3PO_4. Similarly, Zhou et al.[13] prepared a series of $Ag_3PO_4/MgFe_2O_4$ composites with different amounts of $MgFe_2O_4$. The composite with 10 wt % of $MgFe_2O_4$ increased the efficiency of the photocatalytic degradation of RhB under visible light, with the reaction rate constant being 2 times higher than that of the pure sample. These studies attributed the increase in the photocatalytic efficiency to the synergic effect between the semiconductors that resulted in efficient separation of the electron−hole pairs. The studies on other binary composites produced similar results.[10,14,15] The AgNi5 composite synthesized in this study showed a similar behavior with the addition of a small amount of NiO (only 5 mol %), while the addition of higher amounts of NiO lowered the photocatalytic efficiency.

To investigate the possible photocatalytic mechanism of Ag_3PO_4, AgNi5, and AgNi75, isopropanol (IPA), *p*-benzoquinone (BQ), and ammonium oxalate (AO) were utilized as scavengers for hydroxyl radicals ($OH^•$), superoxide radicals ($O_2^{•-}$), and holes (h^+), respectively. Figure 8a shows that the degradation efficiency of Ag_3PO_4 in the absence of scavengers was 97.5%. The addition of IPA, BQ, and AO during the photocatalytic process changed the degradation efficiency to 97.5, 87.1, and 19.1%, respectively. These results show that the $OH^•$ and $O_2^{•-}$ radicals are not involved in the photocatalytic mechanism of RhB, while h^+ play a key role. The photocatalytic process of RhB was primarily governed by direct oxidation by h^+, which is in accordance with the literature.[4]

Conversely, the addition of BQ decreased the degradation efficiency of the AgNi5 composite from 97.1 to 76.8%. The degradation efficiency of AgNi5 after the addition of the IPA and AO was similar to that observed for Ag_3PO_4. h^+ was the primary active species that was involved in the photocatalytic mechanism of the AgNi5 composite; $O_2^{•-}$ also contributed, to a lesser extent, to the degradation of the RhB dye (Figure 8b). The primary active species that was involved in the photocatalytic mechanism of the AgNi75 composite was $O_2^{•-}$, followed by h^+. $OH^•$ also contributed to photocatalysis because the addition of IPA decreased the degradation efficiency from 27.2 to 15.8% (Figure 8c). The formation of the composite was therefore fundamental to indirect oxidation by $OH^•$ and $O_2^{•-}$ radicals, which breaks with the limitation of direct charge transfer between h^+ and the dye, which is limited by the RhB adsorption on the Ag_3PO_4 surface. Colored dyes usually absorb some visible light. Therefore, dye photosensitization can indirectly cause the degradation of RhB under visible light when vigorous adsorption occurs on the surface of the semiconductor. However, previous reports show that the intrinsic photocatalytic degradation of RhB is higher than that of dye photosensitization of RhB.[16]

The positions of the CB and VB in the semiconductors play an important role in the elucidation of the photocatalytic mechanism of the Ag_3PO_4/NiO composite. The CB potential (E_{CB}) and VB potential (E_{VB}) were theoretically estimated according to the following equations (eqs 1 and 2)[56,57]

$$E_{CB} = \chi - E_0 - 0.5E_{gap} \quad (1)$$

$$E_{VB} = E_{CB} + E_{gap} \quad (2)$$

where E_{gap} is the band gap energy of the semiconductor, with experimental values of 2.3 and 2.9 eV for Ag_3PO_4 and NiO, respectively; E_0 is the free-electron energy on the hydrogen scale (approximately 4.5 vs NHE); and χ is the absolute electronegativity of the semiconductor. The χ values for the semiconductors were obtained as the geometric mean of the electronegativities of the constituent atoms, with values of 5.96 and 5.75 eV for Ag_3PO_4 and NiO, respectively.[58,59] Thus, the E_{CB} and E_{VB} of Ag_3PO_4 were 0.31 and 2.6 eV, respectively, while those of NiO were −0.20 and 2.7 eV, respectively, which agrees well with the previous reports.[10,14,25,60] These results are in agreement with those obtained by PL measurement (Figure 6). The composites are of the type-I because the positions of the VB and CB of NiO are lower and higher, respectively, than that of the VB and CB of Ag_3PO_4.[51,52,54,61]

Based on these results, a possible photocatalytic mechanism for the Ag_3PO_4/NiO composite is proposed[62] (Figure 9). Under visible-light irradiation, both Ag_3PO_4 and NiO are excited, generating electron−hole pairs. Because of the relative positions of the bands, the photoexcited e^- in the CB of NiO flows down to the CB of Ag_3PO_4, and the photoexcited h^+ in the VB of NiO also flows to the VB of Ag_3PO_4. Therefore, there is an accumulation of charge in Ag_3PO_4 and a suppression of the recombination processes in NiO.[63,64] In type-I composites, the redox reaction occurs primarily on the surface of the semiconductor in which the charges accumulate.[51,52,61]

Theoretically, the photoexcited e^- cannot react with dissolved O_2 to produce $O_2^{•-}$, as the E_{CB} of Ag_3PO_4 (0.31 eV) is more positive than the potential of couple $O_2/O_2^{•-}$ (−0.18 eV vs NHE).[62,65] However, several recent reports have shown that the accumulated electrons on the surface of Ag_3PO_4 can react with the adsorbed O_2 generate $O_2^{•-}$.[55,66,67] Then, in the composites, $O_2^{•-}$ may be formatted predominantly in the CB of the Ag_3PO_4. Furthermore, the ECB of NiO (−0.2 eV) is slightly more negative than the reduction potential of the couple $O_2/O_2^{•-}$, which suggests that the

https://dx.doi.org/10.1021/acsomega.0c02456
ACS Omega 2020, 5, 21651−21661

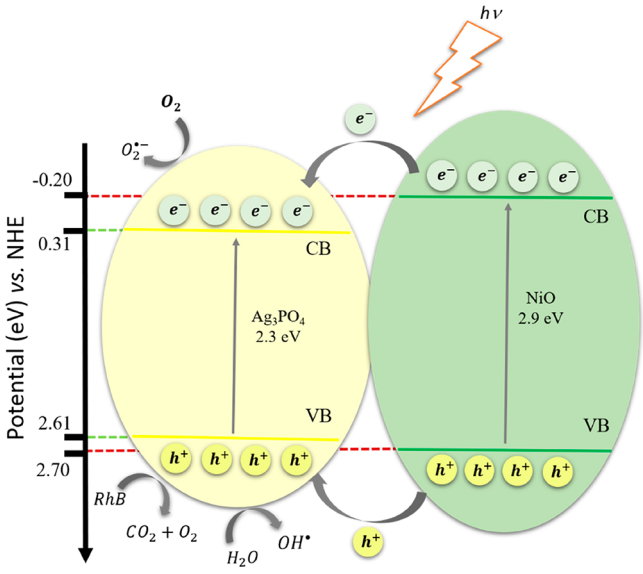

Figure 9. Schematic diagram of band-energy levels with possible photocatalytic mechanism for the Ag_3PO_4/NiO composites under visible-light irradiation.

photoexcited e^- in the CB of NiO could also reduce the dissolved O_2 to $O_2^{\bullet-}$.[68] It was found that for both pure Ag_3PO_4 and the composites, h^+ in the VB of Ag_3PO_4 possessed high reduction potential and could directly oxidize the absorbed RhB molecules. As demonstrated in Figure 8b, the pure Ag_3PO_4 does not oxidize H_2O molecules to $OH^{\bullet}$ radicals. However, the accumulation of h^+ on the surface of Ag_3PO_4 led to the generation of $OH^{\bullet}$ ($OH^{\bullet}/H_2O$; 2.27 eV vs NHE)[62,65] in the photocatalytic mechanism of the AgNi75 composite. These results were consistent with the photocatalytic mechanism observed for the composites (Figure 8b,c).

The increase in the photocatalytic efficiency of the AgNi5 composite might be attributed to an increased capacity to absorb visible light. The band gap of AgNi5 (2.1 eV) was narrower than that of Ag_3PO_4 (2.3 eV), as demonstrated by the DRS analysis (Figure 4c). Moreover, the PL measurements (Figure 6) demonstrated the increase in the photogenerated electrons and holes in the CB and VB of Ag_3PO_4, respectively. These accumulated electron−hole pairs could also react with the absorbed molecules.[52,61] In the AgNi75 composite, the increase in the photogenerated electron−hole pairs in Ag_3PO_4 caused its PL response to be better than that of pure NiO. However, the photocatalytic efficiency was limited by the low proportion of Ag_3PO_4 in the composite because the redox reaction occurs primarily on the Ag_3PO_4 surface.

The structural stabilities of Ag_3PO_4, AgNi5, and AgNi75 were evaluated by performing three consecutive photocatalytic tests. The recycling test with the pure NiO sample was not performed because of its low photocatalytic performance. Figure S3 shows that Ag_3PO_4 and AgNi5 presented a similar behavior with loss of activity of 22.1 and 27.7% after the third cycle, respectively. The photocatalytic efficiencies of AgNi5 and pure Ag_3PO_4 decreased to a similar extent after recycling (Figure S3). However, the AgNi75 sample maintained the photocatalytic efficiency after three cycles. It lost only 2.8% of its activity after the third cycle. The AgNi75 sample, which possessed the highest concentration of NiO among all composites, exhibited the lowest charge recombination, as demonstrated by the PL measurement. This was evidenced by the low PL intensity that probably suppressed the photocorrosion ($Ag^+ + e^- \rightarrow Ag^0$) reaction, thereby influencing the stability and photocatalytic response.

CONCLUSIONS

In summary, NiO microflowers with a narrowed band gap of 2.9 eV were successfully prepared by a hydrothermal method. From this sample, a new visible light-driven Ag_3PO_4/NiO photocatalytic composite was obtained by a simple in situ precipitation method, as confirmed by XRD and Rietveld refinement. The FE-SEM morphologies showed that the composite is formed by NiO microflowers in contact with Ag_3PO_4 microparticles. The photocatalytic efficiencies of the AgNi5 and AgNi25 composites were higher than that of pure Ag_3PO_4 due to the synergistic effect between Ag_3PO_4 and NiO phases in the composites. There was interaction between the phases with NiO acting as a charge carrier donor for Ag_3PO_4, thereby increasing the photogeneration of the electron−hole pairs in the Ag_3PO_4/NiO composites. Moreover, there was enhanced visible-light absorption, as demonstrated by the DRS analysis resulting from the appropriate band-energy levels of the Ag_3PO_4/NiO composites. In these samples, direct oxidation by photoexcited holes is the main active species in the mechanisms. The greater structural stability of the AgNi75 composite was attributed to the low recombination rate of this sample. Based on the present study, it is possible to observe that optimization of the molar ratio of Ag_3PO_4 and NiO in the composites is very important for developing an efficient and stable photocatalyst with activation under visible light.

EXPERIMENTAL SECTION

Synthesis of NiO Powders. The NiO powders were prepared via a simple hydrothermal method, an adaptation of the synthetic route described by Liu et al.[28] In a typical experiment, 0.5995 g of nickel nitrate hexahydrate [$Ni(NO_3)_2 \cdot 6H_2O$] (Sigma-Aldrich, 97%) and 0.3640 g of urea [$(NH_2)_2CO$] (Nox Lab Solution, 99%) were solubilized in a solution containing 20 mL of distilled water and 10 mL of ethanol [C_2H_5OH] (Cromoline, 99%). This solution was transferred into a Teflon reactor of a stainless steel autoclave with an internal volume of 50 mL. The reactor was maintained at 120 °C for 12 h, generating a green precipitate, which was washed with distilled water and ethanol. The obtained material was dried at 80 °C for 12 h and calcined at 400 °C for 2 h, generating a dark-colored solid.

Synthesis of Ag_3PO_4/NiO Composites. The Ag_3PO_4/NiO composites were obtained by an in situ precipitation process. For this, a set amount of the as-synthesized NiO sample was added to 75 mL of distilled water and sonicated for 10 min to obtain a uniform suspension. Then, 3 mmol silver nitrate ($AgNO_3$, Sigma-Aldrich, 99%) was added to the suspension under constant agitation. Subsequently, 25 mL of a solution of diammonium hydrogen phosphate [$(NH_4)_2HPO_4$, Sigma-Aldrich, 98%] also was added dropwise to the suspension, maintaining the stoichiometric molar ratio of $AgNO_3$ and $(NH_4)_2HPO_4$ (3:1). The resulting suspension was maintained under constant agitation for 1 h. The obtained material was washed with distilled water and ethanol and dried at 60 °C for 12 h. Composites with various amounts of NiO were prepared by altering the amount of NiO added initially. The composites with various molar ratios of NiO (5, 25, 50, and 75%) to Ag_3PO_4 are denoted AgNi5, AgNi25, AgNi50,

https://dx.doi.org/10.1021/acsomega.0c02456
ACS Omega 2020, 5, 21651−21661

and AgNi75, respectively. For comparison, pure Ag_3PO_4 was also prepared under the same conditions without adding NiO.

Characterization Techniques. The samples were characterized by XRD with a PANalytical Empyrean diffractometer using Cu Kα (λ = 1.5406 Å) radiation. The measurements were performed under 50 kV and 100 mA with a scanning speed of 0.02°/s in the 2θ range from 10 to 90°. The Rietveld refinements were performed using the GSAS software package with the EXPGUI graphical interface. The theoretical diffraction pattern adopted in the refinements were taken from ICSD no. 14000 (Ag_3PO_4)[30] and no. 9866 (NiO).[31] FTIR was performed on a PerkinElmer IR Spectrum Two spectrophotometer in the transmission mode with a resolution of 4 cm^{-1} using KBr pellets. The spectra were obtained in the range from 400 to 4000 cm^{-1}. Micro-Raman spectroscopy was carried out using a Horiba Jobin-Yvon iHR550 spectrometer coupled to a CCD detector and an argon-ion laser (Melles Griot) operating at 514 nm. The spectra were measured in the range from 70 to 1200 cm^{-1}. UV−vis DRS was performed on a Varian model Cary 5G spectrophotometer in the range from 200 to 800 nm. The morphologies were analyzed using a Carl Zeiss Supra 35-VP field-emission scanning electron microscope operated at 5 kV. PL measurements were carried out on a spectrometer (Ocean Optic-QE65000) with a helium cadmium (HeCd) laser, (Kimmon-IK5451R-E) which emits at 442 nm. The incident laser beam power on the sample was maintained at 50 mW, and all measurements were realized at room temperature.

Photocatalytic Measurements. The photocatalytic activity of the samples was investigated by discoloration of RhB (Sigma-Aldrich, 99%) dye under visible light in a photo-reactor with six Philips TL-D 75/650 fluorescents tubs (15 W), with emission from 400 to 680 nm, operating at 20 °C. In these measurements, 0.030 g of each photocatalyst was added to 50 mL of RhB aqueous solution (5.0 $mg{\cdot}L^{-1}$) and sonicated for 10 min. This suspension was maintained in the dark for 30 min to reach sorption−desorption equilibrium. Subsequently, during the irradiation time, 3 mL of the RhB aqueous solution was removed at defined time intervals (1, 3, 5, 7, 10, 15, 20, 25, and 30 min) and centrifuged to remove the photocatalyst from the solution. Finally, the concentration of RhB was determined by absorbance measurements at 554 nm using a UV−vis spectrophotometer. The photolysis of RhB, without catalyst, was realized following the same experimental procedure described above.

The recycling experiments were performed for three consecutive photocatalytic tests under the same conditions to evaluate the structural stability. After each photocatalytic activity test, with 30 min of exposure to the visible-light irradiation, the suspension was centrifuged to recycle the solids, which were washed with distilled water and ethanol and then dried at 60 °C for 12 h for further testing. Additionally, the reactive species present during the photocatalytic process were investigated by the addition of radical scavengers, such as IPA ($(CH_3)_2CHOH$, 98%, Êxodo), BQ ($C_6H_4O_2$, 98%, Sigma-Aldrich), and AO ($(NH_4)_2C_2O_4{\cdot}H_2O$, 99%, Dinâmica).[69] Before illuminating the mixtures, 0.05 mmol of each scavenger was added to the RhB solution, and these tests were performed under the same conditions mentioned above.

■ ASSOCIATED CONTENT

Supporting Information

The Supporting Information is available free of charge at https://pubs.acs.org/doi/10.1021/acsomega.0c02456.

Atomic coordinates obtained from Rietveld refinements of the pure samples; bond angles and lengths of the pure samples; Rietveld refinement parameters of Ag_3PO_4/NiO composites; UV−Vis DRS absorbance spectra and insets showing digital photos of all samples, and photocatalytic results of three consecutive photocatalytic tests (PDF)

■ AUTHOR INFORMATION

Corresponding Author

Gleice Botelho − *Department of Environmental Chemistry, Federal University of Tocantins, Gurupi, Tocantins 77402-970, Brazil;* orcid.org/0000-0002-7591-1381; Email: gleice.lorena@uft.edu.br

Authors

Ricardo K. Santos − *Department of Environmental Chemistry, Federal University of Tocantins, Gurupi, Tocantins 77402-970, Brazil*

Tiago A. Martins − *CDMF-UFSCar, Federal University of São Carlos, São Carlos, São Paulo 13565-905, Brazil*

Gabriela N. Silva − *Department of Environmental Chemistry, Federal University of Tocantins, Gurupi, Tocantins 77402-970, Brazil*

Marcus V. S. Conceição − *Department of Environmental Chemistry, Federal University of Tocantins, Gurupi, Tocantins 77402-970, Brazil*

Içamira C. Nogueira − *Department of Physics, Federal University of Amazonas, Manaus, Amazonas 69077-000, Brazil*

Elson Longo − *CDMF-UFSCar, Federal University of São Carlos, São Carlos, São Paulo 13565-905, Brazil;* orcid.org/0000-0001-8062-7791

Complete contact information is available at: https://pubs.acs.org/10.1021/acsomega.0c02456

Author Contributions

The manuscript was written through contributions of all authors. All authors have given approval to the final version of the manuscript. These authors contributed equally.

Notes

The authors declare no competing financial interest.

■ ACKNOWLEDGMENTS

The authors thank the Coordenação de Aperfeiçoamento de Pessoal de Nível Superior—Brazil (CAPES), Financial Code 001 for financially supporting this research. The authors also thanks Prof. Maximo S. Li for the PL analyses.

■ REFERENCES

(1) Yi, Z.; Ye, J.; Kikugawa, N.; Kako, T.; Ouyang, S.; Stuart-Williams, H.; Yang, H.; Cao, J.; Luo, W.; Li, Z.; Liu, Y.; Withers, R. L. An orthophosphate semiconductor with photooxidation properties under visible-light irradiation. *Nat. Mater.* **2010**, *9*, 559−564.

(2) Zhai, H.; Yan, T.; Wang, P.; Yu, Y.; Li, W.; You, J.; Huang, B. Effect of chemical etching by ammonia solution on the microstructure and photocatalytic activity of Ag_3PO_4 photocatalyst. *Appl. Catal., A* **2016**, *528*, 104−112.

(3) Al Kausor, M.; Gupta, S. S.; Chakrabortty, D. Ag_3PO_4-based nanocomposites and their applications in photodegradation of toxic organic dye contaminated wastewater: review on material design to performance enhancement. *J. Saudi Chem. Soc.* **2020**, *24*, 20−41.
(4) Martin, D. J.; Liu, G.; Moniz, S. J. A.; Bi, Y.; Beale, A. M.; Ye, J.; Tang, J. Efficient visible driven photocatalyst, silver phosphate: performance, understanding and perspective. *Chem. Soc. Rev.* **2015**, *44*, 7808−7828.
(5) Chong, R.; Cheng, X.; Wang, B.; Li, D.; Chang, Z.; Zhang, L. Enhanced photocatalytic activity of Ag_3PO_4 for oxygen evolution and Methylene blue degeneration: Effect of calcination temperature. *Int. J. Hydrogen Energy* **2016**, *41*, 2575−2582.
(6) Botelho, G.; Andres, J.; Gracia, L.; Matos, L. S.; Longo, E. Photoluminescence and photocatalytic properties of Ag_3PO_4 microcrystals: an experimental and theoretical investigation. *ChemPlusChem* **2016**, *81*, 202−212.
(7) Pereira, W. d. S.; Sczancoski, J. C.; Calderon, Y. N. C.; Mastelaro, V. R.; Botelho, G.; Machado, T. R.; Leite, E. R.; Longo, E. Influence of Cu substitution on the structural ordering, photocatalytic activity and photoluminescence emission of $Ag_{3-2x}Cu_xPO_4$ powders. *Appl. Surf. Sci.* **2018**, *440*, 61−72.
(8) Wang, F.-R.; Wang, J.-D.; Sun, H.-P.; Liu, J.-K.; Yang, X.-H. Plasmon-enhanced instantaneous photocatalytic activity of Au@Ag_3PO_4 heterostructure targeted at emergency treatment of environmental pollution. *J. Mater. Sci.* **2017**, *52*, 2495−2510.
(9) Xie, X.; Mao, C.; Liu, X.; Tan, L.; Cui, Z.; Yang, X.; Zhu, S.; Li, Z.; Yuan, X.; Zheng, Y.; Yeung, K. W. K.; Chu, P. K.; Wu, S. Tuning the bandgap of photo-sensitive polydopamine/Ag_3PO_4/graphene oxide coating for rapid, noninvasive disinfection of implants. *ACS Cent. Sci.* **2018**, *4*, 724−738.
(10) Guo, J.; Shi, H.; Huang, X.; Shi, H.; An, Z. AgCl/Ag_3PO_4: A stable Ag-Based nanocomposite photocatalyst with enhanced photocatalytic activity for the degradation of parabens. *J. Colloid Interface Sci.* **2018**, *515*, 10−17.
(11) Shaveisi, Y.; Sharifnia, S. Deriving Ag_3PO_4-CaO composite as a stable and solar light photocatalyst for efficient ammonia degradation from wastewater. *J. Energy Chem.* **2018**, *27*, 290−299.
(12) Ma, P.; Yu, Y.; Xie, J.; Fu, Z. Ag_3PO_4/CuO composites utilizing the synergistic effect of photocatalysis and Fenton-like catalysis to dispose organic pollutants. *Adv. Powder Technol.* **2017**, *28*, 2797−2804.
(13) Zhou, T.; Zhang, G.; Ma, P.; Qiu, X.; Zhang, H.; Yang, H.; Liu, G. Efficient degradation of rhodamine B with magnetically separable Ag_3PO_4@$MgFe_2O_4$ composites under visible irradiation. *J. Alloys Compd* **2018**, *735*, 1277−1290.
(14) Lu, J.; Wang, Y.; Liu, F.; Zhang, L.; Chai, S. Fabrication of a direct Z-scheme type WO_3/Ag_3PO_4 composite photocatalyst with enhanced visible-light photocatalytic performances. *Appl. Surf. Sci.* **2017**, *393*, 180−190.
(15) Saud, P. S.; Pant, B.; Ojha, G. P.; Kim, D.-U.; Kuk, Y.-S.; Park, S.-J.; Park, M.; Kim, H.-Y. One-pot synthesis of Ag_3PO_4/MoS_2 nanocomposite with highly efficient photocatalytic activity. *J. Environ. Chem. Eng.* **2017**, *5*, 5521−5527.
(16) Guo, J.; Ouyang, S.; Zhou, H.; Kako, T.; Ye, J. Ag_3PO_4/$In(OH)_3$ composite photocatalysts with adjustable surface-electric property for efficient photodegradation of organic dyes under simulated solar-light irradiation. *J. Phys. Chem. C* **2013**, *117*, 17716−17724.
(17) Paulose, R.; Mohan, R.; Parihar, V. Nanostructured nickel oxide and its electrochemical behaviour-A brief review. *Nano-Struct. Nano-Objects* **2017**, *11*, 102−111.
(18) Wang, C.; Zhao, Y.; Su, D.; Ding, C.; Wang, L.; Yan, D.; Li, J.; Jin, H. Synthesis of NiO nano octahedron aggregates as high-performance anode materials for lithium ion batteries. *Electrochim. Acta* **2017**, *231*, 272−278.
(19) Zhang, J.; Zeng, D.; Zhu, Q.; Wu, J.; Huang, Q.; Xie, C. Effect of nickel vacancies on the room-temperature NO_2 sensing properties of mesoporous NiO nanosheets. *J. Phys. Chem. C* **2016**, *120*, 3936−3945.
(20) Manikandan, A.; Judith Vijaya, J.; John Kennedy, L. Comparative investigation of NiO nano- and microstructures for structural, optical and magnetic properties. *Phys. E* **2013**, *49*, 117−123.
(21) Ai, L.; Zeng, Y. Hierarchical porous NiO architectures as highly recyclable adsorbents for effective removal of organic dye from aqueous solution. *Chem. Eng. J.* **2013**, *215−216*, 269−278.
(22) Qing, Z.; Haixia, L.; Huali, L.; Yu, L.; Huayong, Z.; Tianduo, L. Solvothermal synthesis and photocatalytic properties of NiO ultrathin nanosheets with porous structure. *Appl. Surf. Sci.* **2015**, *328*, 525−530.
(23) Wan, X.; Yuan, M.; Tie, S.-l.; Lan, S. Effects of catalyst characters on the photocatalytic activity and process of NiO nanoparticles in the degradation of methylene blue. *Appl. Surf. Sci.* **2013**, *277*, 40−46.
(24) Wang, Y.; Zhang, F.; Wei, L.; Li, G.; Zhang, W. Facet-dependent photocatalytic performance of NiO oriented thin films prepared by pulsed laser deposition. *Phys. B* **2015**, *457*, 194−197.
(25) Liang, Z.-Y.; Huang, R.-K.; Liang, R.-W.; Chen, F.; Yu, Y.; Yan, G.-Y. Preparation of a shell nanostructure for highly selective photocatalytic oxidation of organic compounds by wrapping on NiO nanorods exposed {110} facets with ultrathin g-C_3N_4 nanosheets. *Appl. Surf. Sci.* **2019**, *484*, 424−432.
(26) Lin, Z.; Du, C.; Yan, B.; Wang, C.; Yang, G. Two-dimensional amorphous NiO as a plasmonic photocatalyst for solar H_2 evolution. *Nat. Commun.* **2018**, *9*, 4036.
(27) Dubey, P.; Kaurav, N.; Devan, R. S.; Okram, G. S.; Kuo, Y. K. The effect of stoichiometry on the structural, thermal and electronic properties of thermally decomposed nickel oxide. *RSC Adv.* **2018**, *8*, 5882−5890.
(28) Liu, J.; Li, Y.; Ke, J.; Wang, S.; Wang, L.; Xiao, H. Black NiO-TiO_2 nanorods for solar photocatalysis: recognition of electronic structure and reaction mechanism. *Appl. Catal., B* **2018**, *224*, 705−714.
(29) Baygi, N. J.; Saghir, A. V.; Beidokhti, S. M.; Khaki, J. V. Modified auto-combustion synthesis of mixed-oxides TiO_2/NiO nanoparticles: Physical properties and photocatalytic performance. *Ceram. Int.* **2020**, *46*, 15417−15437.
(30) Masse, R.; Tordjman, I.; Durif, A. Refinement of Crystal-Structure of Silver Monophosphate, Ag_3PO_4-Existence of High-Temperature Form. *Z. Kristallogr.* **1976**, *144*, 76−81.
(31) Sasaki, S.; Fujino, K.; Takéuchi, Y. X-ray determination of electron-density distributions in oxides, MgO, MnO, CoO, and NiO, and atomic scattering factors of their constituent atoms. *Proc. Jpn. Acad. Ser. B Phys. Biol. Sci.* **1979**, *55*, 43−48.
(32) Finger, L. W.; Cox, D. E.; Jephcoat, A. P. A correction for powder diffraction peak asymmetry due to axial divergence. *J. Appl. Crystallogr.* **1994**, *27*, 892−900.
(33) Ramasami, A. K.; Reddy, M. V.; Balakrishna, G. R. Combustion synthesis and characterization of NiO nanoparticles. *Mater. Sci. Semicond. Process.* **2015**, *40*, 194−202.
(34) Botelho, G.; Sczancoski, J. C.; Andres, J.; Gracia, L.; Longo, E. Experimental and theoretical study on the structure, optical properties, and growth of metallic silver nanostructures in Ag_3PO_4. *J. Phys. Chem. C* **2015**, *119*, 6293−6306.
(35) Gandhi, A.; Wu, S. Strong deep-level-emission photoluminescence in NiO nanoparticles. *Nanomaterials* **2017**, *7*, 231.
(36) Maniammal, K.; Madhu, G.; Biju, V. Nanostructured mesoporous NiO as an efficient photocatalyst for degradation of methylene blue: structure, properties and performance. *Nano-Struct. Nano-Objects* **2018**, *16*, 266−275.
(37) Ayed, B. Crystal structure and ionic conductivity of $AgCr_2(PO_4)(P_2O_7)$. *C. R. Chim.* **2012**, *15*, 603−608.
(38) Jastrzębski, W.; Sitarz, M.; Rokita, M.; Bułat, K. Infrared spectroscopy of different phosphates structures. *Spectrochim. Acta, Part A* **2011**, *79*, 722−727.
(39) Ma, F.; Yang, Q.; Wang, Z.; Liu, Y.; Xin, J.; Zhang, J.; Hao, Y.; Li, L. Enhanced visible-light photocatalytic activity and photostability of Ag_3PO_4/Bi_2WO_6 heterostructures toward organic pollutant

https://dx.doi.org/10.1021/acsomega.0c02456
ACS Omega 2020, 5, 21651−21661

degradation and plasmonic Z-scheme mechanism. *RSC Adv.* **2018**, *8*, 15853−15862.
(40) Jin, J.; Sun, J.; Lv, K.; Guo, X.; Liu, J.; Bai, Y.; Huang, X.; Liu, J.; Wang, J. Oxygen-Vacancy-Rich BiO_{2-x}/Ag_3PO_4/CNT Composite for Polycyclic Aromatic Hydrocarbons (PAHs) Removal via Visible and Near-Infrared Light Irradiation. *Ind. Eng. Chem. Res.* **2020**, *59*, 5725−5735.
(41) Lacerda, M. M.; Kargar, F.; Aytan, E.; Samnakay, R.; Debnath, B.; Li, J. X.; Khitun, A.; Lake, R. K.; Shi, J.; Balandin, A. A. Variable-temperature inelastic light scattering spectroscopy of nickel oxide: Disentangling phonons and magnons. *Appl. Phys. Lett.* **2017**, *110*, 202406.
(42) Chakhoum, M. A.; Boukhachem, A.; Ghamnia, M.; Benameur, N.; Mahdhi, N.; Raouadi, K.; Amlouk, M. An attempt to study (111) oriented NiO-like TCO thin films in terms of structural, optical properties and photocatalytic activities under strontium doping. *Spectrochim. Acta, Part A* **2018**, *205*, 649−660.
(43) Wang, C.; Zhang, C.; Hua, W.; Guo, Y.; Lu, G.; Gil, S.; Giroir-Fendler, A. Catalytic oxidation of vinyl chloride emissions over Co-Ce composite oxide catalysts. *Chem. Eng. J.* **2017**, *315*, 392−402.
(44) Zhu, W.; Sun, F.; Goei, R.; Zhou, Y. Facile fabrication of RGO-WO_3 composites for effective visible light photocatalytic degradation of sulfamethoxazole. *Appl. Catal., B* **2017**, *207*, 93−102.
(45) Nail, B. A.; Fields, J. M.; Zhao, J.; Wang, J.; Greaney, M. J.; Brutchey, R. L.; Osterloh, F. E. Nickel Oxide Particles Catalyze Photochemical Hydrogen Evolution from Water-Nanoscaling Promotes P-Type Character and Minority Carrier Extraction. *ACS Nano* **2015**, *9*, 5135−5142.
(46) Madhu, G.; Biju, V. Effect of Ni^{2+} and O^{2-} vacancies on the electrical and optical properties of nanostructured nickel oxide synthesized through a facile chemical route. *Phys. E* **2014**, *60*, 200−205.
(47) Wood, D. L.; Tauc, J. Weak absorption tails in amorphous semiconductors. *Phys. Rev. B: Solid State* **1972**, *5*, 3144.
(48) Tolvaj, L.; Mitsui, K.; Varga, D. Validity limits of Kubelka-Munk theory for DRIFT spectra of photodegraded solid wood. *Wood Sci. Technol.* **2011**, *45*, 135−146.
(49) Wang, D.; Yang, P.; Huang, B. Three-dimensional flowerlike iron oxide nanostructures: Morphology, composition and metal ion removal capability. *Mater. Res. Bull.* **2016**, *73*, 56−64.
(50) Song, X.; Li, R.; Xiang, M.; Hong, S.; Yao, K.; Huang, Y. Morphology and photodegradation performance of Ag_3PO_4 prepared by $(NH_4)_3PO_4$, $(NH_4)_2HPO_4$ and $NH_4H_2PO_4$. *Ceram. Int.* **2017**, *43*, 4692−4701.
(51) Ge, J.; Zhang, Y.; Heo, Y.-J.; Park, S.-J. Advanced design and synthesis of composite photocatalysts for the remediation of wastewater: A review. *Catalysts* **2019**, *9*, 122.
(52) da Silva, J. S.; Machado, T. R.; Trench, A. B.; Silva, A. D.; Teodoro, V.; Vieira, P. C.; Martins, T. A.; Longo, E. Enhanced photocatalytic and antifungal activity of hydroxyapatite/α-$AgVO_3$ composites. *Mater. Chem. Phys.* **2020**, *252*, 123294.
(53) da Silva, J. S.; Machado, T. R.; Martins, T. A.; Assis, M.; Foggi, C. C.; Macedo, N. G.; Beltrán-Mir, H.; Cordoncillo, E.; Andrés, J.; Longo, E. α-$AgVO_3$ Decorated by hydroxyapatite ($Ca_{10}(PO_4)_6(OH)_2$): Tuning its Photoluminescence emissions and bactericidal activity. *Inorg. Chem.* **2019**, *58*, 5900−5913.
(54) Oliveira, L. H.; Ramírez, M. A.; Ponce, M. A.; Ramajo, L. A.; Albuquerque, A. R.; Sambrano, J. R.; Longo, E.; Castro, M. S.; La Porta, F. A. Optical and gas-sensing properties, and electronic structure of the mixed-phase $CaCu_3Ti_4O_{12}/CaTiO_3$ composites. *Mater. Res. Bull.* **2017**, *93*, 47−55.
(55) Abroshan, E.; Farhadi, S.; Zabardasti, A. Novel magnetically separable $Ag_3PO_4/MnFe_2O_4$ nanocomposite and its high photocatalytic degradation performance for organic dyes under solar-light irradiation. *Sol. Energy Mater. Sol. Cells* **2018**, *178*, 154−163.
(56) Butler, M. A.; Ginley, D. Prediction of flatband potentials at semiconductor-electrolyte interfaces from atomic electronegativities. *J. Electrochem. Soc.* **1978**, *125*, 228−232.
(57) Ma, Z.; Yi, Z.; Sun, J.; Wu, K. Electronic and photocatalytic properties of Ag_3PC_4VI (C= O, S, Se): a systemic hybrid DFT study. *J. Phys. Chem. C* **2012**, *116*, 25074−25080.
(58) Xu, Y.; Schoonen, M. A. A. The absolute energy positions of conduction and valence bands of selected semiconducting minerals. *Am. Mineral.* **2000**, *85*, 543−556.
(59) Pearson, R. G. Absolute electronegativity and hardness: application to inorganic chemistry. *Inorg. Chem.* **1988**, *27*, 734−740.
(60) Raja, V. R.; Rosaline, D. R.; Suganthi, A.; Rajarajan, M. Ultrasonic assisted synthesis with enhanced visible-light photocatalytic activity of NiO/Ag_3VO_4 nanocomposite and its antibacterial activity. *Ultrason. Sonochem.* **2018**, *44*, 73−85.
(61) Abdullah, H.; Gultom, N. S.; Kuo, D.-H. A simple one-pot synthesis of a Zn (O, S)/Ga_2O_3 nanocomposite photocatalyst for hydrogen production and 4-nitrophenol reduction. *New J. Chem.* **2017**, *41*, 12397−12406.
(62) Bard, A. J.; Parsons, R.; Jordan, J. *Standard Potentials in Aqueous Solution*; CRC Press: New York, 1985; pp 1−848.
(63) Dhanabal, R.; Velmathi, S.; Bose, A. C. High-efficiency new visible light-driven Ag_2MoO_4−Ag_3PO_4 composite photocatalyst towards degradation of industrial dyes. *Catal. Sci. Technol.* **2016**, *6*, 8449−8463.
(64) Wang, H.; Zhang, L.; Chen, Z.; Hu, J.; Li, S.; Wang, Z.; Liu, J.; Wang, X. Semiconductor heterojunction photocatalysts: design, construction, and photocatalytic performances. *Chem. Soc. Rev.* **2014**, *43*, 5234−5244.
(65) Koppenol, W. H.; Stanbury, D. M.; Bounds, P. L. Electrode potentials of partially reduced oxygen species, from dioxygen to water. *Free Radical Biol. Med.* **2010**, *49*, 317−322.
(66) Yang, X.; Tang, H.; Xu, J.; Antonietti, M.; Shalom, M. Silver phosphate/graphitic carbon nitride as an efficient photocatalytic tandem system for oxygen evolution. *ChemSusChem* **2015**, *8*, 1350−1358.
(67) Ghazalian, E.; Ghasemi, N.; Amani-Ghadim, A. R. Enhanced visible light photocatalytic performance of Ag_3PO_4 through doping by different trivalent Lanthanide cations. *Mater. Res. Bull.* **2017**, *88*, 23−32.
(68) Xu, Y.-S.; Zhang, W.-D. Monodispersed Ag_3PO_4 nanocrystals loaded on the surface of spherical Bi_2MoO_6 with enhanced photocatalytic performance. *Dalton Trans.* **2013**, *42*, 1094−1101.
(69) Chu, C.-Y.; Huang, M. H. Facet-dependent photocatalytic properties of Cu_2O crystals probed by using electron, hole and radical scavengers. *J. Mater. Chem. A* **2017**, *5*, 15116−15123.

https://dx.doi.org/10.1021/acsomega.0c02456
ACS Omega 2020, 5, 21651−21661